Electronic transport and consequences for material removal in ultrafast pulsed laser ablation of materials

N. M. Bulgakova
Institute of Thermophysics SB RAS, 1 Acad. Lavrentyev Avenue, 630090 Novosibirsk, Russia

R. Stoian,* A. Rosenfeld, and I. V. Hertel
Max-Born-Institut für Nichtlineare Optik und Kurzzeitspektroskopie, Max-Born Strasse 2a, D-12489 Berlin, Germany

E. E. B. Campbell
Department of Experimental Physics, Göteborg University and Chalmers University of Technology, SE-41296 Göteborg, Sweden
(Received 8 September 2003; published 9 February 2004)

Fast electronic transport is investigated theoretically based on a drift-diffusion approach for different classes of materials (metals, semiconductors, and dielectrics) under ultrafast, pulsed laser irradiation. The simulations are performed at intensities above the material removal threshold, characteristic for the ablation regime. The laser-induced charging of dielectric surfaces causes a subpicosecond electrostatic rupture of the superficial layers, an effect which, in comparison, is strongly inhibited for metals and semiconductors as a consequence of superior carrier transport properties.

DOI: 10.1103/PhysRevB.69.054102 PACS number(s): 79.20.Ds, 52.50.Jm

I. INTRODUCTION

The importance of carrier dynamics in ultrafast laser ablation of materials has been indicated on numerous occasions,[1–6] and the study of electronic transport in irradiated solid samples has the potential of elucidating the strong differences observed in the material removal characteristics for different classes of materials irradiated under similar conditions.[7] As an example, a rather rough but widely accepted estimation for laser-induced optical damage in nonconducting materials is based on a modified Boltzmann transport formalism. This results in a quantified description for free-electron generation, depending on the laser energy input and on the crude assumption that damage occurs whenever the normally weakly absorbing solid develops strong absorbing characteristics.[8] In other words, the occurrence of the optically induced destruction of the initially transparent material depends on reaching a critical electron density at which resonant collective electronic oscillations occur, and on the effectiveness of the energy coupling into the laser-induced electron-hole plasma.

Since the theoretical description of carrier dynamics in dielectric and semiconductor targets under high-intensity pulsed laser irradiation or electron beam bombardment is rather complicated, the topic has not been covered thoroughly. By convention, existing models may be divided into three groups, depending on the preferred approach. In Refs. 3 and 9–11, carrier dynamics in silicon targets was studied in the frame of ambipolar diffusion with an implicit assumption of an equal number of electrons and holes in the solid and preservation of local quasineutrality of the sample. Another approach, developed for semiconductors irradiated by laser pulses[12] and dielectrics under the action of electron beams,[13,14] takes into account the generation of local electric fields inside the target with the assumption that the target remains neutral as a whole. This implies the absence of electron photoemission[12] or relies on secondary electron emission equal to the absorbed electron flux.[13,14] In Ref. 13, the concept of a double layer (DL) was applied to processes involving particle-beam–matter interactions to describe the spatial charge arrangement in the bulk of the irradiated material. It should be stressed though that the irradiation regimes considered in Refs. 12–14 are far below material breakdown. A third approach proposed in Refs. 15 and 16 for the case of a dielectric target (MgO) irradiated by a laser pulse of nanosecond duration may be labeled as the drift-diffusion approach. The authors studied the self-consistent generation of an electric field as a result of laser heating of the electrons excited to the conduction band, their diffusion, and drift in the locally established fields. The possibility of electron emission is considered, involving at the same time the lifting of the constraint of target neutrality. The calculated local electric field is found to reach values exceeding 10^8 V/m under normal ablation conditions. The above-mentioned models are suitable for nonconducting or poorly conducting materials. For ultrafast pulsed laser irradiated metals using pulse durations shorter than the characteristic times for electron energy loss,[17–22] the most utilized model is based on the assumption of two interacting systems (electrons and lattice) characterized by different laser-induced initial temperatures and exchanging energy on a time scale set by the electron-lattice interactions.

Recent studies at irradiation intensities above the damage threshold have pointed out the potential of solid charging to induce an electrostatic disintegration of the surface following efficient photoelectron emission.[7,23] The occurrence of the surface Coulomb explosion (CE) generating macroscopic material removal and high ion kinetic energies has been demonstrated for dielectrics,[7] while for semiconductors and metals[24] the subject remains controversial.

The paper is organized as follows. Section II introduces the main characteristics of the calculation model, emphasizing also specific features for metals, dielectrics, and semiconductors. Section III discusses the consequences derived from

the calculations and provides a comparison between the different types of materials used as model systems. It outlines the effects of the fast electronic transport in ultrafast laser irradiation and their relevance for laser ablation. A main result predicts that, within the range of the calculated irradiation doses, surface macroscopic Coulombic explosion can take place only for dielectric materials.

II. MODEL

In this work we investigate the role of electron-related processes responsible for generating specific paths that lead to material ejection under ultrafast laser irradiation. The questions we try to answer refer to the role of neutrality breakdown related to the charge carrier distribution in different types of excited solids, the magnitude, the duration of this disequilibrium, and its influence on the material removal characteristics. We have used a simplified drift-diffusion continuum approach to model the energy flow into the sample in the first hundreds of femtoseconds of the interaction, in a restricted region, confined within a few hundred nanometers beneath the surface. Our attempt is aimed at providing a common simplified frame applicable to different kinds of materials (dielectrics, semiconductors, and metals) under ultrashort pulsed laser irradiation and discussing the importance of photoelectron emission in generating totally nonthermal material ejection mechanisms. The unified approach is justified by a similar plasmalike behavior when high excitation densities are generated by high-power ultrafast laser irradiation sources.[25,26] For all three classes of materials, the model is based on solving the following equations.

(a) The continuity equation for the evolution of the laser-generated charge carriers

$$\frac{\partial n_x}{\partial t}+\frac{1}{e}\frac{\partial J_x}{\partial x}=S_x+L_x, \tag{1}$$

where the two terms on the right-hand side represent sources (S) for carrier production and losses (L) in the laser-generated carrier population, and n_x denotes the carrier densities with subscript $x=e$, i representing electrons and ions, respectively.

(b) The equation of motion describing the transport of charge in a locally established electric field E, with the electric current density[16] J including both drift and diffusion terms,

$$J_x=|e|n_x\mu E-eD\nabla n_x. \tag{2}$$

The time- and space-dependent diffusion coefficient D is calculated, if not otherwise mentioned, as $D=k_BT_x\mu_x/e$, where T_x represents the carrier temperature and μ_x is the carrier mobility.

(c) The Poisson equation to calculate the electric field E generated as a result of locally breaking the quasineutrality inside the irradiated target:

$$\frac{\partial E}{\partial x}=\frac{e}{\varepsilon\varepsilon_0}(n_i-n_e). \tag{3}$$

Moreover, the calculations are based on the following assumptions.

(i) Laser excited metals and highly ionized nonconducting materials are considered as dense plasmas[25,26] with similar properties.

(ii) The zero-field material properties are considered equal at the interface and in the bulk.

(iii) The laser electric field does not influence the macroscopic electron drift within the charged region.

(iv) The electronic flow is caused by quasineutrality violation on and beneath the target surface due to electron photoemission and strong density gradients.

The system of equations (1)–(3) was solved assuming the targets are irradiated using a near-infrared ultrafast laser pulse with a Gaussian temporal profile. Since we are focusing on a reduced zone of a few hundred nm, we do not account for the small spatial extent of the laser pulse and propagation effects[27] and, therefore, the intensity profile is written as

$$I(t)=[1-R(t)]\frac{2F_0}{\tau_L}\sqrt{\frac{\ln 2}{\pi}}\exp\left[-4\ln 2\left(\frac{t}{\tau_L}\right)^2\right], \tag{4}$$

where F_0 is the incident laser fluence, the laser pulse duration is $\tau_L=100$ fs (full width at half maximum), and R is the time-dependent reflection coefficient. All the calculations were performed for a laser radiation wavelength of $\lambda=800$ nm corresponding to the most encountered experimental situations in ultrafast laser material processing. A one-dimensional model justified by enhanced transverse lateral dimensions for the laser spot with respect to the absorption depth has been employed. Every set of equations has its own features dictated by material properties. Particular situations for individual classes of materials will be discussed below.

Modeling was performed for the one-dimensional case using an explicit numerical scheme. The targets—gold (Au), silicon (Si), and sapphire (Al_2O_3)—used as model systems for different material classes are divided into 5-Å-thick layers (numerical cells). Whenever possible, the model parameters follow the general characteristics of different material classes rather than underlining particular properties of the selected materials. The electric current density was calculated at the cell boundaries, whereas the other parameters were calculated in the center of the cells. The depth of the numerical region was chosen in such a way that further increase did not essentially influence the numerical results, still ensuring that the one-dimensional approach was valid. In the remote bulk boundary (with respect to the target surface), the condition of free-electron flow was applied. A cell was added above the target surface to simulate the vacuum conditions, and the electric field at the target surface was calculated using Gauss' law.

Special attention was paid to carefully choosing the time step. As the electric field reaches values above 10^{10} V/m, leading in turn to high electron drift velocities, the time step required is extremely small, thus resulting in a large calculation time. Because of the free flow condition set for the remote (bulk) boundary, there was no possibility to accurately control the conservatism of the numerical scheme. In order

to find adequate time steps providing a good approximation to the problem, the input equations were initially solved with the limiting condition of zero electric field at the bulk boundary. This implies that the photoemitted electrons remain in the vicinity of the surface during the laser pulse, so that a capacitor type of structure is generated: the positively charged solid layer depleted of electrons and the photoelectron layer above the surface. Moreover, setting zero electric field and restricting diffusion (one may do this because of the small electron density gradient) in the remote boundary, the conservation of the number of electrons can be easily controlled. It was found that, with a 10-attoseconds step, the number of electrons is conserved with good precision up to electric field values at the target surface on the order of 10^8 V/m, whereas at higher fields conservation breakdown will result in a strong increase in the electron number with respect to the number of ions. Thus, decreasing the time step for electric fields above 10^8 V/m is necessary for successful modeling. The above-determined time steps were then implemented in the calculation where the condition of free electronic flow together with Gauss' equation define the true value of the field at the remote boundary.

A. Metals

The continuity equation for free electrons [Eq. (1)] in a metal target (gold in our case) is assumed to contain no source terms. It is understood implicitly that fast thermalization within the electronic system occurs so that the two-temperature model remains valid. It has to be added though that fluence-dependent, delayed electronic thermalization with sub-ps time scales has been observed several times.[28,29] At the surface, photoemission was treated in the form of a boundary condition for the three-photon generated electron current density,[30–35] describing the interfacial electron flow into the vacuum. Three photons are necessary, at our photon energy of 1.55 eV, to overcome the potential barrier and to release the electron into the vacuum. The three-photon photoemission cross section c_{Au}, containing the relevant information about the electron escape probability, escape depth, and energy gain, was empirically determined[30,31] by measuring the total electronic charge emitted in the irradiation process. We correct this for the absorption changes corresponding to the present irradiation wavelength (800 nm). The nanosecond pulse durations used for investigations in Refs. 30 and 31 are not likely to raise the electronic temperature significantly. However, ultrafast, sub-ps irradiation of metals is able to induce extremely high electronic temperatures, in the range of 1 eV, while the lattice remains cold for the time scales of interest. This makes imperative the correction for temperature-dependent effects, based on the generalized Fowler-DuBridge theory for multiphoton photoemission at high temperatures.[32–35] At high irradiation intensities (few TW/cm^2) around and above the damage threshold at the lattice melting temperature, the thermally assisted three-photon photoemission will be the major contribution to the promotion of electrons above the vacuum level. Additionally, the thermal contribution (neglecting space-charge effects[36,37]) to the ejected electron flux has been considered in the form of the Richardson-Duschman equation,[36] so that the total emitted electron current density takes the form below. The thermal emission of high-temperature electrons will play a more important role during the tail of the laser pulse where the energy stored into the electronic system reaches a maximum value,

$$J_e|_{x=0} = c_{\mathrm{Au}} \frac{2(kT_e)^2}{(3\hbar\omega-\varphi)^2} F\left(\frac{3\hbar\omega-\varphi}{kT_e}\right)(1-R)^3 I^3 + A_0 T_e^2 \exp\left(-\frac{\varphi}{kT_e}\right), \tag{5a}$$

with

$$c_{\mathrm{Au}} \approx \frac{ep\,\delta_{\mathrm{PE}}}{\hbar\omega\left(3a_{\mathrm{Au}}+\frac{1}{l_{\mathrm{PE}}}\right)} \propto \frac{a_{3-\mathrm{Au}}}{2}\left(\frac{e}{\hbar\omega}\right)^3\left(\frac{3\hbar\omega-\varphi}{k}\right)^2. \tag{5b}$$

Here I is the laser intensity, A_0 is the theoretical Richardson coefficient (120 A/cm^2 K^2), φ is the barrier height for electron promotion into vacuum, k is the Boltzmann constant, T_e is the electronic temperature (considered to be position-independent within the electron escape region), and R is the reflectivity. F represents the Fowler function described in Refs. 32–35. $a_{3-\mathrm{Au}}$ is a coefficient describing the three-photon contribution to the photoemission process, e is the electron charge, p is the electron escape probability, $\hbar\omega$ is the incident photon energy (1.55 eV), a_{Au} is the metal absorption coefficient at the laser wavelength, and l is the electron escape depth ($\sim$5 nm[30]). δ_{PE} is the part of the three-photon absorption coefficient ending above the vacuum level and resulting in electron photoemission, which has been corrected for the present wavelength based on considerations related to the electronic population and accessible density of states below the Fermi level. A parabolic description of the band energy versus the density of states,[38] characteristic of the free-electron case, was used and the region accessible to three-photon excitation was written with respect to the Fermi level as

$$\int_{E_F-(3\hbar\omega-\varphi)}^{\infty} \frac{E^{1/2}}{\exp[(E-E_F)/kT_e+1]}\,dE.$$

The spatial and temporal behavior of the free-electron temperature that influence both the strength of photoemission and the diffusion efficiency are governed by the heat-flow equation,[20]

$$A_e\left(\frac{\partial}{\partial t}(T_e^2)+\frac{J}{en_e}\frac{\partial}{\partial x}(T_e^2)\right) = \frac{K_{e,0}}{T_l}\frac{\partial^2}{\partial x^2}(T_e^2)+2\Sigma(x,t), \tag{6}$$

where the indexes e,l refer to the electron and lattice parameters, respectively, $A_e = C_e/T_e$ with C_e being the electronic heat capacity, and the thermal conductivity of the electrons K_e is introduced as a temperature-dependent quantity equal to $K_{e,0}T_e/T_l$.[20] The heat transport equation accounts for both heat conductivity and direct, bulk, or across the vacuum

TABLE I. Modeling parameters for gold.

Parameters	Value
Electron specific heat constant A_e	71 ($J\,m^{-3}\,K^{-2}$)[a]
Electronic thermal conductivity $K_{e,0}$	318 ($W\,m^{-1}\,K^{-1}$)[a]
Absorption depth λ_0 (at 800 nm)	14.4×10^{-9} (m)[b]
Ballistic range λ_{ball}	1.05×10^{-7} (m)[a]
Reflection coefficient R	0.949[c]
Electron mobility μ	5.17×10^{-3} ($m^2\,V^{-1}\,s^{-1}$)[d]
Work function ϕ	4.25 (eV)[c]

[a]Reference 20.
[b]Reference 40.
[c]Reference 41.
[d]Reference 42.

interface electronic transport from the excited region (e.g., due to photoemission, which has the additional role of removing hot electrons from the irradiated surface and subsequently supplying the interaction region with cold bulk electrons). Ballistic effects for electronic energy transport in the first $\sim$100 nm, which are significant in noble metals, have been considered through the action of an effective absorption depth in the source term that more efficiently redistributes the laser energy within the ballistic range of the electron transport.[20] The time scale of interest for the considered process is less than 1 ps, so that electron-lattice relaxation may be neglected and the lattice temperature is assumed to be constant. The energy source term in Eq. (6) is written as in Refs. 20 and 21,

$$\Sigma(x,t)=I_0(t)(1-R)\frac{\exp[-x/(\lambda_0+\lambda_{ball})]}{(\lambda_0+\lambda_{ball})}, \tag{7}$$

where λ_0 is the optical-absorption depth and λ_{ball} is the ballistic range for the hot electrons. No transient reflectivity changes during the laser pulse at increasing electron energy have been taken into account, keeping the effect of interband transitions minimal.[21,39] Higher-order nonlinear contributions to light absorption and attenuation, as well as additional three-body collisional processes for hot electron production, were also not considered.

In contrast to dielectric and semiconductor targets, where laser radiation penetrates into a considerable depth at the beginning of the laser pulse (because of a low intensity, weakly absorbed leading edge), for a metal target the region perturbed by radiation (skin depth) is on the order of 0.5 μm. In this specific region, rapid heating of the electronic system takes place and strong electron-lattice nonequilibrium is induced. Due to high electron thermal conductivity and heat diffusion outside the irradiated region, the affected region widens rapidly. To meet these requirements, at the beginning of the calculations a relatively small computational region is chosen ($\sim$1.5–2 μm). At the bulk boundary, the following conditions are set: unperturbed electron temperature ($T_{e0}=300$ K), quasineutrality ($n_e=n_i$), and free, nonrestricted electron in-flow. During the calculations, the numerical region was expanded. To account for this, at a boundary point of $N-5$, where N is the total number of grid points, a temperature control is performed with the criterion $(T_e-T_{e0})/T_e\leqslant10^{-4}-10^{-5}$ for each time step. Whenever this condition was not fulfilled anymore, the number of the grid points was increased. At the interface, the condition $(\partial T_e/\partial x)=0$ is set to indicate that there is no heat transfer through the interface except for the energy carried away by the emitted electrons.

The modeling parameters used for the gold target[20,40–42] are given in Table I.

B. Dielectrics

In a dielectric material (i.e., sapphire), the source and loss terms in Eq. (1) for electrons can be written as

$$S_e=(W_{mph}+Q_{av})\frac{n_a}{n_a+n_i} \tag{8}$$

and

$$L_e=-R_e-X_{PE}. \tag{9}$$

It is implicitly assumed that diffusion as well as energy transport follow almost instantly the establishment of the density or temperature gradients according to the Fourier law, an assumption that may have a reduced degree of validity under ultrafast, nonequilibrium situations involving a considerable amount of energy input.

In Eq. (8), $W_{mph}=\sigma_6 I^6$ is the rate of a six-photon ionization process corresponding to an energy band gap of approximately 9 eV, n_a is the density of neutral atoms, $Q_{av}=\alpha I n_e$ is the avalanche term,[8] R_e represents the linear decay term accounting for recombination and trapping processes, and X_{PE} denotes the photoelectron emission. Both source terms are corrected for the reduction in the density of ionization centers (neutral atoms providing the electronic reservoir of the valence band) during photoionization. The diffusion coefficient D [Eq. (2)] was calculated with the assumption that the average electron energy in the conduction band is approximately 5 eV.[8,43] In the calculations, to compensate for the mobility decay with temperature, a simplified, time-independent diffusion coefficient was used. The multiphoton ionization cross section σ_6 and avalanche coefficient α were based on a fit to the experimental results for the optical dam-

age threshold at different pulse durations[44] following a similar approach to that of Ref. 8, taking also into consideration the observed decay in the threshold electron density for longer pulse durations.[45] The multiphoton ionization cross section and the avalanche coefficient were estimated for Al_2O_3 as $\sigma_6 = 8\times10^9\ \mathrm{cm}^{-3}\,\mathrm{ps}^{-1}(\mathrm{cm}^2/\mathrm{TW})^6$ and $\alpha = 6\ \mathrm{cm}^2/\mathrm{J}$. The fit-based approach, frequently encountered in ultrafast laser ablation studies,[46,47] can give a better description of any realistic situation. However, for the purpose of this paper, iterating the multiphoton and the avalanche coefficients in order to reach the critical density at the conditions observed in the experiment is not expected to influence the results significantly.[48,49]

The spatially and temporally dependent laser power inside the dielectric target is mainly determined by loss mechanisms involving free-electron generation and by the optical response of a collisional free-electron plasma and the vacuum-plasma interface through the Fresnel formulas. The complex dielectric function at the incident frequency can be seen as a mutual contribution of the unexcited solid and the response of the laser-induced free-electron gas and is given by[8,50]

$$\varepsilon_\omega^*(n_e) \cong 1 + (\varepsilon_g - 1)\left(1 - \frac{n_e}{n_0}\right) - \frac{n_e}{n_{\mathrm{cr}}}\frac{1}{1 + i\dfrac{1}{\omega\tau}}. \quad (10)$$

Here $\varepsilon_\omega^*(n_e)$ represents the complex dielectric function of the excited material, ε_g is the dielectric constant of the unexcited material at the incident wavelength [$\varepsilon_g = n^{1/2} = 3.0983$ (Ref. 51)], and n_e, $n_{\mathrm{cr}} = \varepsilon_0 m_e \omega^2/e^2$, and n_0 are the density of the conduction-band electrons, the critical density for the free-electron gas at 800 nm, and the valence-band electron density, respectively. The effective electronic mass was taken to be equal to the mass of the free electron in vacuum.

To take into account reflection, a scheme with a moving vacuum-plasma interface towards the bulk following electron depletion in the surface layers due to the photoelectric effect, and a multilayered, steplike, inhomogeneous electron density profile[4,50] was applied. The local intensity in a cell is given by the superposition of the direct irradiation and backscattered radiation. The energy balance is written below, where $I(x,t)$ is the local intensity,

$$\frac{\partial}{\partial x} I(x,t) = -W_{\mathrm{mph}}\frac{n_a}{(n_a + n_i)}\hbar\omega n_{\mathrm{ph}} - a_e(x,t) I(x,t). \quad (11)$$

Here n_{ph} is the number of photons required for multiphoton ionization ($n_{\mathrm{ph}} = 6$ to overcome the energy band gap) and ω is the frequency of laser radiation. The free-electron absorption coefficient $a_e(x,t)$ [$a_e = 4\pi/\lambda\ (\frac{1}{2}\{-\mathrm{Re}(\varepsilon^*) + [\mathrm{Re}(\varepsilon^*)^2 + \mathrm{Im}(\varepsilon^*)^2]^{1/2}\})^{1/2}$] is calculated from the complex dielectric response[8] of a collisionally damped free-electron plasma, considering a damping term $\omega\tau = 3$ to match the observed reflectivities of $\sim 70\%$ reported in Ref. 52 for supercritical electron densities generated by high-intensity radiation. No dependences of the damping characteristics at increased electronic densities and temperatures were taken into account.

With regard to the photoemission term, for a quantitative estimation we assume a statistical distribution of free electronic momenta in a wide-band-gap dielectric where the vacuum level lies close to the conduction-band minimum, and only electrons with a momentum component normal to and in the direction of the surface can escape into the vacuum. The minimal energetic distance between the vacuum level and the conduction-band edge, within one photon range (1.55 eV), is a valid assumption for a large class of wide-band-gap materials with weak band-to-band scattering.[53–56] Thus, we assume that, on average, half of the electrons which appear in the processes of multiphoton and avalanche ionization are immediately photoemitted from the surface and below-surface region, taking into account an instantaneously established angular distribution for the carrier momenta. Due to the specific form of the PE term, at significant above-threshold fluences, whenever the avalanche process stops due to the full ionization of the materials in the subsurface region, further electron heating and photoemission does not take place anymore on the tail of the laser pulse, a situation not present here. At high but still not saturated supercritical densities, on the trailing edge of the laser pulse, the initially dielectric material starts to exhibit a metal-like behavior, and emission from the conduction band may become significant.[57] At lower, close-to-damage fluences, the dominant contribution is derived mainly from valence-band ionization by multiphoton and further collisional processes. Maximum photoemission occurs from the surface with an exponential decrease within the bulk. Thus, the photoemission term X_{PE} was written as[7]

$$X_{\mathrm{PE}} = \tfrac{1}{2}\,(W_{\mathrm{mph}} + Q_{\mathrm{av}})\frac{n_a}{n_a + n_i}\exp(-x/l), \quad (12)$$

where the electronic escape depth l was taken as 1 nm.[58] The integral photoemitted charge calculated as above is in good agreement with reported experimental values for dielectric materials.[59] Charging effects on the work function were not explicitly considered, especially since the photoelectron emission can be regarded as a self-regulating process. Strong and early photoemission would lead to depletion in the electron population just below the surface (within the electron escape depth), inhibiting additional electron generation by collisional ionization processes and, therefore, further delaying photoemission at the end of the pulse. Increasing the surface barrier by charging effects would permit more electrons to remain in the surface region, allowing supplementary generation and, in return, stronger photoemission on the trailing edge of the laser pulse.

The ion density is calculated based on Eq. (1), disregarding photoemission and neglecting hole transport in the bulk. The recombination term was put in a general form as n_e/τ describing mainly trapping-like phenomenon (with $\tau = 1$ ps) rather than a three-body saturable recombination process.

The parameters used for sapphire were as follows: energy band gap $E_g = 9$ eV, atomic density is 1.17×10^{23} cm^{-3}, and electron mobility $\mu = 3 \times 10^{-5}$ m^2/(V s) (ten times lower than reported in Ref. 60) for a better match of the observed diffusivities[14] in laser-induced dense plasmas. A significant decrease of the electron mobility is to be expected at high carrier concentration[61,62] and high field values. To preserve a certain character of simplicity and in the absence of detailed data on these particular aspects of the electron transport, we have preferred to work with a reduced zero-field mobility. Since we consider electronic transport in the local electric field, calculated from the Poisson equation, plasma-screening effects within the bulk material are automatically taken into account.

C. Semiconductors

The model for silicon was based on a similar approach to that for sapphire. The radiation reflection at the vacuum interface and the absorption inside the bulk of a strongly excited semiconductor were similarly described based on the optical signature of the unexcited material and the Drude response of the laser-generated free-electron gas[50] [$\varepsilon_g = 13.46 + i0.048$ (Refs. 63 and 64)]. In analogy to Refs. 3 and 50, one- and two-photon ionization terms as well as collisional carrier multiplication were considered in Eq. (1) for the evolution of the electron density,[65,66]

$$S_e = \left[\left(\sigma_1 + \frac{1}{2}\sigma_2 I \right) \frac{I}{\hbar\omega} + \beta n_e \right] \frac{n_a}{n_a + n_i}, \tag{13}$$

$$L_e = -R_e - X_{\mathrm{PE}}. \tag{14}$$

One-photon and two-photon ionization cross sections (σ_1 and σ_2) were taken from Refs. 64 and 65, respectively ($\sigma_1 = 1021$ cm^{-1}, $\sigma_2 = 10$ cm/GW) and the total atomic number density is 5×10^{22} cm^{-3}. The avalanche electronic multiplication (β), though reduced for silicon[50,67] irradiated with ultrashort pulses (Ref. 67 gives an impact ionization rate in Si well below 10^{14} s^{-1}, approaching gradually at high electron kinetic energies the value reported for dielectrics[68]), has been put in the form given by van Driel.[9] The loss term at low electronic densities $R_e = C n_e^2 n_i$ is mainly determined by an Auger recombination process[9] with $C = 3.8 \times 10^{-31}$ cm^6/s reaching a saturation level at electronic densities approaching 10^{21} cm^{-3}.[4,69] While the carrier population decays via a three-body recombination mechanism, the Auger processes will preserve the energy within the carrier system. At high densities, the decay in the electron population is influenced by a characteristic relaxation time, τ_0.[69] Accordingly,

$$R_e = \frac{n_e}{\tau_0 + 1/C n_e n_i} \tag{15}$$

with $\tau_0 = 6 \times 10^{-12}$ s.[69]

An additional equation for hole generation takes into account the hole transport process.

The current densities for the electrons and holes are based on the following parameters:[38] $\mu_e = 0.015$ m^2/(V s) and $\mu_h = 0.0045$ m^2/(V s), both mobilities being ten times reduced compared to the low carrier density values[38] to account for the reduction at high carrier densities and temperatures.[61,62,70]

Electron photoemission[71] was considered in analogy with the gold sample [Eq. (5)], taking into account a three-photon photoemission event from the conduction band with a corrected coefficient (both for the wavelength and the accessible density of states) with respect to those previously used for Au. To rescale δ_{PE} [Eq. (5b)], a Fermi-Dirac distribution for the free electrons in a parabolic conduction band was considered. Corrections have also been made to account for the dependence of the absorption coefficient on the free-electron density in excited semiconductors.[60,71–73] As ionization of silicon occurs very rapidly at the beginning of the laser pulse, inducing a metal-like state for the considered fluence (0.8 J/cm^2), to describe the physical reality and to avoid the instability of the numerical scheme we scaled the photoemission term to the number of available electrons n_e (to account for the variable number of free electrons) normalized to the gold electron density. Instead of the Si work function ($\varphi = 4.6$ eV), an effective potential barrier $\varphi_{\mathrm{eff}} = 4.05$ eV (Ref. 56) given by the initial electronic state and measured from the bottom of the conduction band was introduced as the relevant parameter.

The emitted electron current is the sum of the photoemission from the conduction band and a thermal ionization term:

$$J_e|_{x=0} \propto X_{\mathrm{PE_{CB}}} + X_{\mathrm{PE_{Th}}}, \tag{16}$$

$$J_e|_{x=0} = \left[c_{\mathrm{Au}} \frac{\delta_{\mathrm{PE\text{-}Si}}}{\delta_{\mathrm{PE\text{-}Au}}} \frac{\left(3a_{\mathrm{Au}} + \frac{1}{l_{\mathrm{PE\text{-}Au}}} \right)}{\left(3a_{e\text{-}\mathrm{Si}} + \frac{1}{l_{\mathrm{PE\text{-}Si}}} \right)} \times \frac{2(kT_e)^2 (1-R)^3 I^3}{(3\hbar\omega - \varphi_{\mathrm{eff}})^2} F\left(\frac{3\hbar\omega - \varphi_{\mathrm{eff}}}{kT_e} \right) + A_0 T_e^2 \exp\left(-\frac{\varphi_{\mathrm{eff}}}{kT_e} \right) \right] \frac{n_{e\text{-}\mathrm{Si}}}{n_{e\text{-}\mathrm{Au}}}. \tag{17}$$

The contribution of four-photon photoelectron emission from the valence band was not considered, as it is too small in comparison with the main contribution from the conduction band.[56]

The spatial and temporal distribution of the laser intensity in the sample was calculated as

$$\frac{\partial}{\partial x} I(x,t) = -\left(\sigma_1 \frac{n_a}{n_a + n_i} + \sigma_2 \frac{n_a}{n_a + n_i} I(x,t) + a_{e\text{-}\mathrm{Si}}(x,t) \right) I(x,t) \tag{18}$$

with $I(0,t) = [1 - R(t)] I_0(t) - (3\hbar\omega/e) J_e|_{x=0}$, taking into account one- and two-photon ionization, inverse bremsstrahlung absorption of light by the laser-induced free electrons in

the conduction band, as well as losses due to the three-photon photoemission. Higher-order processes were not considered for absorption, as their effect is negligible.[56] Simultaneously, the energy deposited and transported in the free electronic system interacting with the lattice was calculated by balancing the absorbed amount of photons in the following equations:

$$\frac{\partial E_f}{\partial t} = \left((\hbar\omega - E_g)\frac{\sigma_1 I}{\hbar\omega} + (2\hbar\omega - E_g)\frac{\sigma_2}{2}\frac{I^2}{\hbar\omega} - E_g \beta n_e \right) \times \frac{n_a}{n_a + n_i} + a_{e\text{-Si}} I(x,t) + E_g R_e , \tag{19a}$$

$$A_e\left(\frac{\partial T_e}{\partial t} + \frac{J}{e n_e}\frac{\partial T_e}{\partial x}\right) = \frac{\partial}{\partial x}K_e\frac{\partial T_e}{\partial x} - \frac{A_e}{\tau}(T_e - T_l) + \frac{2}{3n_e}\frac{\partial E_f}{\partial t}, \tag{19b}$$

$$A_l\frac{\partial T_l}{\partial t} = \frac{\partial}{\partial x}K_l\frac{\partial T_l}{\partial x} + \frac{A_e}{\tau}(T_e - T_l). \tag{19c}$$

The parameters have the following designations: E_f, the energy of the full electron system in a numerical cell; $E_e = E_f/n_e$, the average energy of one electron; T_e, the electron temperature, $T_e = 2E_e/3k$; T_l, the lattice temperature. Heat capacity and thermal conductivity, respectively, are taken as $A_e = \frac{3}{2}k$ and $K_e = 4k^2(\mu_e T_e/e)$.[9,74] A_e/τ describes the energy coupling to the lattice and the hot carrier relaxation time was taken as $\tau = \tau_R[1 + (n_e/n_{cr})^2]$ with $\tau_R = 240$ fs.[65]

Since the optical signature of a free electronic gas approximates very well the behavior of the excited Si sample,[50] absorption and reflection coefficients were calculated by a Drude-type scheme for a collisionally damped electron-hole plasma induced by an ultrashort laser pulse (100 fs) at normal incidence ($R_{(t=-\infty)} = 0.34$),[51,64] in a similar manner to the approach used for dielectric materials.

III. RESULTS AND DISCUSSION

The models were initially tested by calculating the damage thresholds for gold, silicon, and sapphire and comparing them with previously published data. The heat-transfer equation [Eq. (6)] for metals is suitable to describe the electronic subsystem heating on the femtosecond time scale, but it is invalid for a time domain when electron-lattice exchange becomes significant. In order to extend the thermal transport calculation for gold up to the melting time, the complete two-temperature problem for heat propagation[20] was solved for our irradiation conditions

$$C_e\left(\frac{\partial T_e}{\partial t} + \frac{J}{e n_e}\frac{\partial T_e}{\partial x}\right) = \frac{\partial}{\partial x}K_e\frac{\partial T_e}{\partial x} - g(T_e - T_l) + \Sigma(x,t), \tag{20a}$$

$$C_l\frac{\partial T_l}{\partial t} = \frac{\partial}{\partial x}K_l\frac{\partial T_l}{\partial x} + g(T_e - T_l). \tag{20b}$$

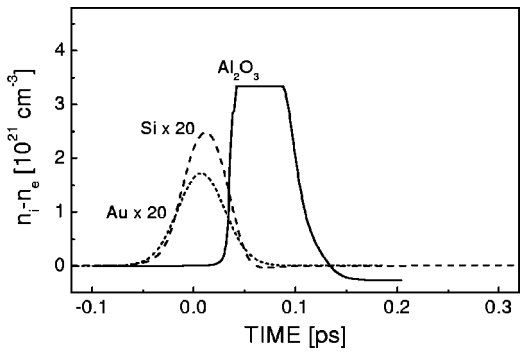

FIG. 1. Calculations of the net charge density (the difference between the electron and hole populations, respectively) located at the surface as a function of the laser time for different classes of materials under investigation. Laser fluences are chosen to be above the ion emission threshold for each material ($F_{Al_2O_3} = 4$ J/cm^2, $F_{Si} = 0.8$ J/cm^2, $F_{Au} = 1.2$ J/cm^2). The laser pulse is centered at $t = 0$.

Here C_e, C_l, K_e, and K_l are heat capacities and thermal conductivities of electrons and lattices, respectively, and g is the electron-lattice coupling constant. Melting of a 1-μm film is reached at an incident fluence of 0.93 J/cm^2 (equivalent to 0.047 J/cm^2 absorbed fluence), in agreement with previous observations.[7,20] The damage thresholds for Si and sapphire take place when electronic densities in excess of 10^{21} cm^{-3} are reached, at 0.3 and 2.7 J/cm^2, respectively, also in good agreement with the experimental studies.[44,47,75] According to the model, the Si sample experiences a thermodynamic solid-to-liquid phase transition and starts to melt at around 0.5 J/cm^2, a value higher than those experimentally reported,[75] since the hole contribution to phonon generation was not explicitly accounted for.[76] It should be stressed that numerical results on damage thresholds do not depend significantly on whether photoemission was taken into account or not. Considerable electron depletion of the surface layer of the sapphire target leads only to a slight shift of the breakdown region (i.e., overcritical electron densities) towards the bulk (on the order of the electronic escape depth).

The results of the calculations related to the buildup and decay of a net positive charge on the surface of samples representative for different classes of materials (Al_2O_3, Si, and Au) are plotted in Fig. 1 as a function of time. The laser fluences used to calculate the charging dynamics are slightly above the experimental ion emission thresholds,[20,44–47,50] namely 4 J/cm^2 for Al_2O_3, 0.8 J/cm^2 for Si, and 1.2 J/cm^2 for Au, respectively. Under these specific irradiation conditions, the electronic temperature reaches high values ranging from around 1 eV in gold to approximately 5 eV in silicon and even more in sapphire. It is obvious that the net charge is significantly higher for the dielectric target than for the metal or for the semiconductor target. Sufficient charge can be accumulated at the dielectric surface on the 100-fs time scale that creates an electrostatic stress with magnitudes comparable to the mechanical binding strength, and thus initiates the surface Coulombic explosion. It should be emphasized that strong charging of sapphire illustrated in Fig. 1 is not a result of higher photoemission, as compared to silicon and gold. The sapphire target loses approximately 6.8×10^8 elec-

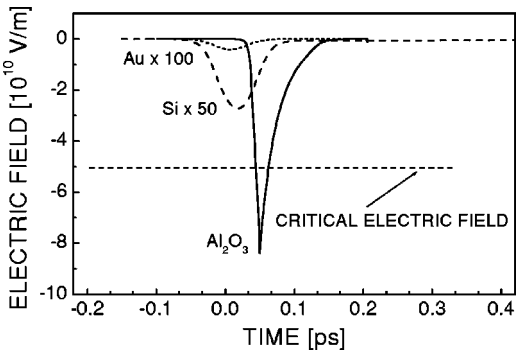

FIG. 2. Temporal behavior of the induced electrostatic field in the surface region of the sample for all three classes of materials under investigation. In the dielectric case the field survives over the critical threshold for a few tens of fs. For metals and semiconductor, the charge-induced electrostatic field remains well below the material break-up threshold value.

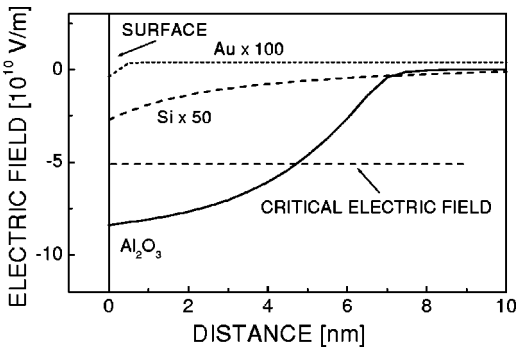

FIG. 3. Spatial bulk profile of the electric field induced in metals, semiconductors, and dielectrics.

trons over the whole laser pulse duration from an irradiated spot of 470 μm^2, whereas 6.9×10^{11} and 3.5×10^{11} electrons are removed from Si and Au targets, respectively.

We have estimated the threshold value of the electric field necessary to break the atomic bonds in sapphire. The cubic energy density of the electric field is expressed as $w=\varepsilon\varepsilon_0E^2/2$. The value $W_{at}=\varepsilon\varepsilon_0E^2V_{at}/2$ is the energy of the electric field corresponding to one atom in the crystal, where V_{at} is the volume occupied by a single atom in the crystal, $V_{at}=n^{-1}$. The energy necessary to remove an atom from the target can be estimated from the latent heat of sublimation calculated for a single atom, $\Lambda_{sub}=485.7$ kJ/mol,[42] which corresponds to approximately 5 eV. Thus, the threshold electric field is of the order of

$$E_{th}|_{x=0}=\sqrt{\frac{2\Lambda_{at}}{\varepsilon\varepsilon_0V_{at}}}=\sqrt{\frac{2\Lambda_{at}n}{\varepsilon\varepsilon_0}}, \tag{21}$$

where n is the number density. For sapphire we obtain $E_{th}\sim5\times10^{10}$ V/m. Figure 2 shows the temporal behavior of the net electric field developed at the sapphire surface in comparison with the field values induced in other types of materials. The negative value implies that the field is directed away from the target, streaming from the subsurface layers to the vacuum. It can be observed that the electric field exceeds the critical value and reaches a value of 8.4×10^{10} V/m at the surface. The above-threshold electric field exists for a few tens of fs. The spatial distribution of the electric field in the near-surface layers is given in Fig. 3 at a time of 50 fs after the maximum of the laser pulse, when the electrostatic field has reached its top value. The layer with overcritical electric field where electrostatic disintegration of the lattice should occur is approximately 40 Å wide, in excellent agreement with the experimental estimation of the Coulomb exploded region.[23]

With semiconductors and metals, the higher electron mobility and higher density of available free electrons ensure effective screening and a much smaller net positive charge accumulated during the laser pulse, in spite of the fact that for the Si sample, supercritical carrier densities are reached. This is not sufficient to induce a macroscopic electrostatic break-up of the outer layers of the substrate. The maximum values of the electric field are only 4.1×10^7 V/m and 5.4×10^8 V/m for gold and silicon, respectively.

Returning to Fig. 1, we will discuss in the following the effect of the size of the numerical region. In the case of a gold target, the size of the numerical region is determined by the heat-flow equation, and increasing the region does not influence the results of the calculations. For silicon targets, the only condition which should be met requires that in the remote boundary, the number of free electrons should correspond to the intrinsic population at room temperature of 1.5×10^{10} cm^{-3}.[38] For sapphire, due to the transparency of the initial state and ionization along the laser propagation, the situation is more complex. At any time the free-electron density is decreasing in the remote boundary as this moves away from the target surface. This occurrence has far-reaching consequences. Namely, the value of the generated free-electron density determines the supply efficiency of the numerical region with electrons, accounting for the value of the electric field and net charging. Numerical regions of 0.1 and 10 μm can be considered the two extreme, limiting cases. In the first case, a high electron density in the remote boundary is generated, resulting in a fast supply of the electrons to the surface layer. This involves a more intense avalanche causing higher maximum charging, however the surface electric field still does not reach the critical value estimated above, lying just below the breakdown threshold. The size of 10 μm corresponds to the irradiated spot radius in the experiments[7,23] and indicates the limit of the one-dimensionality. Further increasing the calculated slab implies a strong violation of the problem dimension and therefore necessitates accounting for lateral electron supply to the central part of the irradiated spot. Starting from the numerical region of 1 μm, the maximum charging is similar to the solid curve shown in Fig. 1 (given for 1 μm) but the period of maximum charging increases as the remote boundary moves deeper in the bulk.

The charge dynamics are strongly correlated with the absorption characteristics for each of the materials (Fig. 1). There is a quite different behavior for sapphire when compared to the other materials. The charging is retarded, instead of roughly following the laser pulse envelope, as for metals and semiconductors. The effect is mainly due to electron

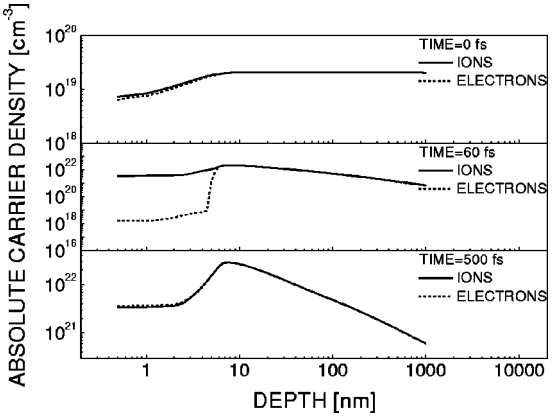

FIG. 4. Spatial profile of the free-electron and ion densities generated in the dielectric sample at different times during and after irradiation.

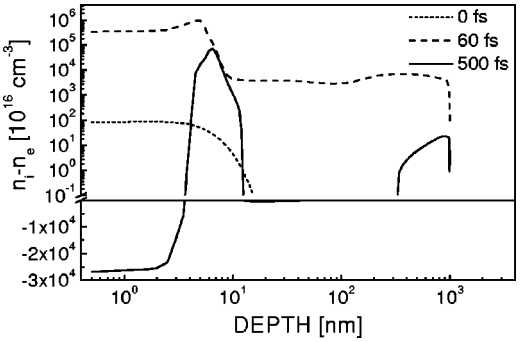

FIG. 5. Spatial depth profiles of the net induced charge density in the dielectric target indicating also the regions susceptible to be affected by Coulomb explosion.

heating and collisional multiplication taking place during the tail of the laser pulse, thus being directly linked to the number of free electrons in the surface layers. As follows from the calculations, a sapphire sample irradiated by a laser pulse with a fluence of 4 J/cm^2 accumulates multiphoton-generated seed electrons during the first half of the pulse. Only when the electron density reaches a value on the order of $10^{17}-10^{18}$ cm^{-3} does avalanche start to dominate over multiphoton ionization in the calculated regime, leading to the subsequent dielectric breakdown. At this point very efficient electron heating and photoemission occurs, resulting in supercritical surface charging. An additional factor that will significantly increase the electron energy at the end of the laser pulse at high input fluences is the drastic reduction of the available number of neutral atoms that can serve as electron sources for collisional multiplication. The electron avalanche fades away and its importance in removing energy from the electronic degrees of freedom ceases.

As discussed above, the electric field in the first cell below the surface reaches a value of $\sim 8.4\times 10^{10}$ V/m. An external field $E_{\mathrm{ex}}=\varepsilon E_{\mathrm{in}}$ is established in front of the surface. The accumulated electrostatic stress determines the surface disruption and the emitted ions will be driven by the field for a few tens of fs (characteristic time of the electric field ''pulse'' in Fig. 2) and subsequently accelerated. The final momentum obtained by the ion subject to the action of the electric field E_{ex} during time τ is written as $Mv=eE_{\mathrm{ex}}\tau$, where M is the ion mass. This gives an estimate of the maximum velocity acquired by an Al^+ ion of $v\geqslant 10^4$ m/s that closely agrees with the value detected in time-of-flight experiments.[23] During the time when considerable surface charging exists, the ions travel a distance on the order of a few tens of Å. Thus, the charged surface layer is destroyed within an interval of several tens of femtoseconds.

The spatial distributions of both carrier density and the accumulated net charge in the near-surface regions for the sapphire target are presented in Figs. 4 and 5 for different times with respect to the maximum of the laser pulse. The results demonstrated here have been obtained with a simulated region of 1-μm thickness. At $t=0$ fs (Fig. 4), corresponding to the peak of the laser pulse, breakdown conditions have not yet been reached (critical electron density for the laser-induced free-electron gas for the case considered is 1.74×10^{21} cm^{-3}), neither at the surface nor in the neighboring regions. Due to photoemission, the external layer of the target is strongly depleted of electrons, resulting in lower avalanche and, hence, in decreased ionization of the residual neutrals. The dielectric is ionized to a considerable depth due to the penetration of the leading edge of the laser pulse. At this point, the laser-induced surface charging is weak and electron diffusion has not yet developed, so that only a surface layer a few tens of an Å thick is positively charged (the difference in the density profiles of electrons and ions is almost unnoticeable in the figure).

The critical electron density in the surface layer is reached about 25 fs after the pulse maximum, the ionization process develops further in a skin layer where 20% ionization is reached approximately 20 fs later (see Fig. 4 for $t=60$ fs), and the magnitude of the surface charge levels out. Dielectric breakdown develops within a region of 350 nm, whereas considerable positive charging (from 3% to 10% of atomic density) in the lattice arises in a superficial layer of only 60-Å thickness (Fig. 5). One can see that maximum charging is reached at a distance of 50 Å under the target surface. However, despite higher charging than in the first 40-Å layer, Coulomb explosion in the maximum charging region is improbable because of the subcritical electric field value (see Fig. 3). Note that, due to depletion of the outer layer of electrons, the reflection interface has moved towards the bulk (~ 60 Å).

The electric field is directed towards the vacuum in the surface layer of 60-nm thickness (Fig. 3) and changes sign in the deeper regions. Thus, in a thin surface layer there is a competition between electron drift directed towards the bulk and diffusion tending to fill the layer depleted of electrons. In the deeper regions the situation is the opposite. A steep gradient of the electronic density leads to electron diffusion towards the bulk, whereas the drift component of the electron current is directed towards the surface, tending to fill the positive charge space region present due to electron photoemission. The two main processes responsible for the charge redistribution result in a double-layer effect,[13] similar to that developed in expanding plasmas.[77,78] However, this effect is weak during the laser pulse and only becomes pronounced at later times.

The carrier redistribution picture is strongly nonstationary during the laser irradiation. During the tail of the laser pulse, continuing photoemission and the corresponding redistribution of the components of the electronic current result in further changing of the charge distributions. Approximately 100 fs after the laser pulse termination, the process reaches a certain quasiequilibrium between the opponent drift and diffusion terms, with a slight variation in time due to possible electronic decay channels (recombination at traps, self-trapping, Auger recombination) and electron supply from the bulk.

Such a quasistationary picture is given in Fig. 5 (500 fs after the laser peak). Since the direct photoemission process has stopped, the electron current from the bulk is gradually closing the charged gap near the surface. Despite the negative surface layer, a certain quantity of net positive charge still exists in the subsurface zone with a higher degree of ionization and determines a region of maximum electron density from where the electrons stream to the less-ionized regions due to diffusion (Fig. 5). Due to the attraction generated by the narrow positive subsurface layer, a region with electron excess arises in the less-ionized interface region. Figure 5 illustrates the picture of a classic double layer.[13,77,78] Note that the peak of positive charge is approximately three times higher than that of the negative surface charge and it is followed by a wider region with reduced negative charge load. In even deeper regions where the electron density gradients are small, drift in the direction of the surface is the main contribution to the electron current and a new positive area is formed but with a smaller net charge density.

The spatial description of the charge transport into the volume (Fig. 5) of the dielectric material at different times shows that indeed only during the first 100 femtoseconds is it possible to generate significant electrostatic removal; after that the charge is slowly redistributed in the bulk. Interestingly, a succession of positively and negatively charged layers (double layer) appears with the ability to screen the bulk redistributed charge. A notable consequence of photoemission, which can take place for both dielectrics and semiconductors subjected to laser irradiation, is lower ionization in a thin superficial target layer, so that the breakdown region shifts towards the bulk. For the cases when the avalanche mechanism contributes considerably to breakdown development, this displacement effect seems to be inevitable. Since the subsurface target layer is less strongly ionized than the deeper region, one expects that this layer will be charged negatively at later times. This happens at ~ 0.13 ps when the net charge drops below zero, as can be seen in Fig. 1. When the electric field drops below $\sim 5\times 10^9$ V/m, the diffusion term in this region starts to dominate the drift and electrons rush to the surface layer.

We have elucidated the main tendencies of electronic transport in the dielectric targets that can result in electrostatic disintegration (Coulomb explosion) of the surface layer. Further development of the presented model including energetic considerations is underway. The temporal behavior of the energy accumulated in the electronic degrees of freedom is of particular interest. Preliminary calculations have shown that the electron average energy rises slowly at the beginning of the laser pulse due to laser field acceleration of the electrons created by the multiphoton ionization of the valence band. A slight energy decrease is evident at the point where avalanche becomes the dominant process for additional free-electron generation by removing energy from the accumulated electronic kinetic energy. A substantial rise in the electron energy appears when the solid is highly ionized and the avalanche alone is not capable anymore of converting energy into further ionization.

Another question of interest concerns the electrons emitted from the target. Here we assume that they instantly disappear from the near-surface zone. However, on femtosecond time scales a substantial portion of such electrons has no time to move to a large distance. The upper limit of the effect of the photoemitted electrons on target charging can be considered by putting the condition of a zero electric field at the remote (bulk) boundary. The calculations have shown that in such a situation with otherwise identical parameters, the maximum electric field increases by less than 1.4 times. Thus, taking into account the electric field generated by the photoelectrons only increases the chances for fast ion ejection from the target. However, it should be underlined that the present theoretical consideration has shown that the Coulomb explosion conditions can be realized even without the electron driving force.

IV. CONCLUSIONS

In conclusion, we have studied theoretically the role of rapid electronic transport in defining the characteristics of material removal with ultrashort laser pulses. A strong electrostatic ion repulsion force causes the break-up of the surface of charged dielectric materials, while for semiconductors and metals efficient neutralization occurs and ablation receives a more thermal appearance. The developed models are general and can be used to describe charge transport dynamics in different materials on ultrafast time scales, accounting also for some of the nonthermal channels experimentally observed in ultrafast laser ablation of materials.

ACKNOWLEDGMENT

The Wissenschaftlich-Technologischen Zusammenarbeit (WTZ) project RUS01/224 is gratefully acknowledged.

*Corresponding author. Electronic mail: stoian@mbi-berlin.de
Also at National Institute for Laser, Plasma and Radiation Physics, Bucharest, Romania.

[1] G. Petite, P. Daguzan, S. Guizard, and P. Martin, Nucl. Instrum. Methods Phys. Res. B **107**, 97 (1996).
[2] M. Li, S. Menon, J. P. Nibarger, and G. N. Gibson, Phys. Rev. Lett. **82**, 2394 (1999).
[3] S. S. Mao, X. L. Mao, R. Greif, and R. E. Russo, Appl. Surf. Sci. **127–129**, 206 (1998).
[4] M. C. Downer and C. V. Shank, Phys. Rev. Lett. **56**, 761 (1986).
[5] M. Bonn, D. N. Denzler, S. Funk, M. Wolf, S. Wellershoff, and J. Hohlfeld, Phys. Rev. B **61**, 1101 (2000).

[6] R. Stoian, M. Boyle, A. Thoss, A. Rosenfeld, G. Korn, E. E. B. Campbell, and I. V. Hertel, Appl. Phys. Lett. **80**, 353 (2002).
[7] R. Stoian, A. Rosenfeld, D. Ashkenasi, I. V. Hertel, N. M. Bulgakova, and E. E. B. Campbell, Phys. Rev. Lett. **88**, 097603 (2002).
[8] B. C. Stuart, M. D. Feit, S. Herman, A. M. Rubenchik, B. W. Shore, and M. D. Perry, Phys. Rev. B **53**, 1749 (1996).
[9] H. M. van Driel, Phys. Rev. B **35**, 8166 (1987).
[10] E. J. Yoffa, Phys. Rev. B **21**, 2415 (1980).
[11] J. F. Young and H. M. van Driel, Phys. Rev. B **26**, 2147 (1982).
[12] T. Held, T. Kuhn, and G. Marler, Phys. Rev. B **44**, 12 873 (1991).
[13] A. Melchinger and S. Hofmann, J. Appl. Phys. **78**, 6224 (1995).
[14] A. Miotello and M. Dapor, Phys. Rev. B **56**, 2241 (1997).
[15] R. M. Ribeiro, M. M. D. Ramos, A. M. Stoneham, and J. M. Correia Pires, Appl. Surf. Sci. **109–110**, 158 (1997).
[16] R. M. Ribeiro, M. M. D. Ramos, and A. M. Stoneham, Thermophys. Aeromechanics **5**, 223 (1998).
[17] S. I. Anisimov, B. Kapeliovich, and T. L. Perel'man, Sov. Phys. JETP **39**, 375 (1974).
[18] M. I. Kaganov, I. M. Lifshitz, and M. V. Tanatarov, Sov. Phys. JETP **4**, 173 (1957).
[19] N. K. Sherman, F. Brunel, P. B. Corkum, and F. A. Hegmann, Opt. Eng. (Bellingham) **28**, 1114 (1989).
[20] S.-S. Wellershoff, J. Hohlfeld, J. Güdde, and E. Matthias, Appl. Phys. A: Mater. Sci. Process. **69**, S99 (1999).
[21] J. Hohlfeld, S.-S. Wellershoff, J. Güdde, U. Conrad, V. Jähnke, and E. Matthias, Chem. Phys. **251**, 237 (2000).
[22] T. Juhasz, H. E. Elsayed-Ali, G. O. Smith, C. Suarez, and W. E. Bron, Phys. Rev. B **48**, 15 488 (1993).
[23] R. Stoian, D. Ashkenasi, A. Rosenfeld, and E. E. B. Campbell, Phys. Rev. B **62**, 13 167 (2000).
[24] E. G. Gamaly, A. V. Rode, B. Luther-Davies, and V. T. Tikhonchuk, Phys. Plasmas **9**, 949 (2002).
[25] S. Nolte, B. N. Chichkov, H. Welling, Y. Shani, K. Lieberman, and H. Terkel, Opt. Lett. **24**, 914 (1999).
[26] D. F. Price, R. M. More, R. S. Walling, G. Guethlein, R. L. Shepherd, R. E. Stewart, and W. E. White, Phys. Rev. Lett. **75**, 252 (1995).
[27] C.-H. Fan and J. P. Longtin, Appl. Opt. **40**, 3124 (2001).
[28] W. S. Fann, R. Storz, H. W. K. Tom, and J. Bokor, Phys. Rev. B **46**, 13 592 (1992).
[29] R. H. M. Groeneveld, R. Sprik, and A. Lagendijk, Phys. Rev. B **45**, 5079 (1992).
[30] E. M. Logothetis and P. L. Hartman, Phys. Rev. Lett. **18**, 581 (1967).
[31] E. M. Logothetis and P. L. Hartman, Phys. Rev. **187**, 460 (1969).
[32] J. H. Bechtel, W. Lee Smith, and N. Bloembergen, Phys. Rev. B **15**, 4557 (1977).
[33] R. Yen, J. Liu, and N. Bloembergen, Opt. Commun. **35**, 277 (1980).
[34] J. P. Girardeau-Montaut and C. Girardeau-Montaut, Phys. Rev. B **51**, 13 560 (1995).
[35] Ph. Martin, R. Trainham, P. Agostini, and G. Petite, Phys. Rev. B **45**, 69 (1992).
[36] X. Y. Wang, D. M. Riffe, Y.-S. Lee, and M. C. Downer, Phys. Rev. B **50**, 8016 (1994).
[37] D. M. Riffe, X. Y. Wang, M. C. Downer, D. L. Fisher, T. Tajima, and J. L. Erskine, J. Opt. Soc. Am. B **10**, 1424 (1993).
[38] R. E. Hummel, *Electronic Properties of Materials* (Springer-Verlag, Berlin, 1993).
[39] C.-K. Sun, F. Vallee, L. H. Acioli, E. P. Ippen, and J. G. Fujimoto, Phys. Rev. B **50**, 15 337 (1994).
[40] V. M. Zolotarev, V. N. Morozov, and E. V. Smirnova, *Optical Constants for Natural and Technical Media* (Khimiya, Leningrad, 1984) (in Russian).
[41] *Physicochemical Properties of the Elements*, edited by G. V. Samsonov (Naukova Dumka, Kiev, 1965) (in Russian).
[42] *Handbook of Physical Quantities*, edited by I. S. Grigoryev, E. Z. Meilikhov, and A. A. Radzig (CRC Press, Boca Raton, FL, 1996).
[43] D. Arnold and E. Cartier, Phys. Rev. B **46**, 15 102 (1992).
[44] D. Ashkenasi, R. Stoian, and A. Rosenfeld, Appl. Surf. Sci. **154–155**, 40 (2000).
[45] F. Quèrè, S. Guizard, P. Martin, G. Petite, O. Gobert, P. Meynadier, and M. Perdrix, Appl. Phys. B: Lasers Opt. **68**, 459 (1999).
[46] M. Lenzner, J. Krüger, S. Santania, Z. Cheng, Ch. Spielmann, G. Mourou, W. Kautek, and F. Krausz, Phys. Rev. Lett. **80**, 4076 (1998).
[47] Ming Li, S. Menon, J. P. Nibarger, and G. N. Gibson, Phys. Rev. Lett. **82**, 2394 (1999).
[48] T. Apostolova and Y. Hahn, J. Appl. Phys. **88**, 1024 (2000).
[49] S. R. Vatsya and S. K. Nikumb, J. Appl. Phys. **91**, 344 (2002).
[50] K. Sokolowski-Tinten and D. von der Linde, Phys. Rev. B **61**, 2643 (2000).
[51] *Handbook of Optics*, edited by W. G. Driscoll and W. Vaughan (McGraw-Hill Book Company, New York, 1978).
[52] D. von der Linde and H. Schüller, J. Opt. Soc. Am. B **13**, 216 (1996).
[53] S. Guizard, P. Martin, and G. Petite, J. Phys.: Condens. Matter **5**, 7033 (1993).
[54] B. Quiniou, W. Schwarz, Z. Wu, R. M. Osgood, and Q. Yang, Appl. Phys. Lett. **60**, 183 (1992).
[55] V. E. Puchin, J. D. Gale, A. L. Shluger, E. A. Kotomin, J. Gunster, M. Brause, and V. Kempter, Surf. Sci. **370**, 190 (1997).
[56] J. G. Mihaychuk, N. Shamir, and H. M. van Driel, Phys. Rev. B **59**, 2164 (1999).
[57] Ph. Daguzan, S. Guizard, K. Krastev, P. Martin, G. Petite, A. Dos Santos, and A. Antonetti, Phys. Rev. Lett. **73**, 2352 (1994).
[58] S. C. Jones, A. H. Fischer, P. Braunlich, and P. Kelly, Phys. Rev. B **37**, 755 (1988).
[59] W. J. Siekhaus, J. H. Kinney, D. Milam, and L. L. Chase, Appl. Phys. A: Solids Surf. **39**, 163 (1986).
[60] R. C. Hughes, Phys. Rev. B **19**, 5318 (1979).
[61] D. Reznik and W. Gerlach, Surf. Sci. Spectra **41**, 405 (1997).
[62] K. Seeger, *Semiconductor Physics, An Introduction*, edited by M. Cardona, P. Fulde, K. Von Klitzig, and H.-J. Queisser, Springer Series in Solid-State Sciences (Springer-Verlag, Berlin, 1991), p. 123.
[63] L. Ward, *The Optical Constants of Bulk Materials and Films* (Institute of Physics Publishing, Bristol, 1994).
[64] T. Y. Choi and C. P. Grigoropoulos, J. Appl. Phys. **92**, 4918 (2002).
[65] T. Sjodin, H. Petek, and H-L. Dai, Phys. Rev. Lett. **81**, 5664 (1998).
[66] D. H. Reitze, T. R. Zhang, Wm. M. Wood, and M. C. Downer, J. Opt. Soc. Am. B **7**, 84 (1990).

[67] E. Cartier, M. V. Fischetti, E. A. Eklund, and F. R. McFeely, Appl. Phys. Lett. **62**, 3339 (1993).
[68] A. Tien, S. Backus, H. Kapteyn, M. Murnane, and G. Mourou, Phys. Rev. Lett. **82**, 3883 (1999).
[69] J. Bok and M. Combescot, Phys. Rev. Lett. **47**, 1564 (1981).
[70] T. Kuhn and G. Mahler, Surf. Sci. Spectra **32**, 1851 (1989).
[71] E. O. Kane, Phys. Rev. **127**, 131 (1962).
[72] C. N. Berglund and W. E. Spicer, Phys. Rev. **136**, A1030 (1964).
[73] G. W. Gobelli, F. G. Allen, Phys. Rev. **127**, 141 (1962).
[74] S. de Unamuno and E. Fogarassy, Appl. Surf. Sci. **36**, 1 (1989).
[75] A. Cavalleri, C. W. Siders, C. Rose-Petruck, R. Jimenez, C. Toth, J. A. Squier, C. P. J. Barty, K. R. Wilson, K. Sokolowski-Tinten, M. H. von Hoegen, and D. von der Linde, Phys. Rev. B **63**, 193306 (2001).
[76] A. Othonos, J. Appl. Phys. **83**, 1789 (1998).
[77] G. Hairapetian and R. L. Stenzel, Phys. Fluids B **3**, 899 (1991).
[78] N. M. Bulgakova, A. V. Bulgakov, and O. F. Bobrenok, Phys. Rev. E **62**, 5624 (2000).